厚生労働科学研究委託費　難治性疾患克服研究事業
（難治性疾患等実用化研究事業（難治性疾患実用化研究事業））

運動失調症の分子病態解明・治療法開発に関する研究
平成26年度　委託事業成果報告書　別冊

業務主任者　水澤　英洋

平成27年（2015年）3月

Acta Neurologica Scandinavica

Acta Neurol Scand DOI: 10.1111/ane.12273

ACTA NEUROLOGICA
SCANDINAVICA

Relationship and factor structure in multisystem neurodegeneration in Parkinson's disease

Hattori T, Orimo S, Hallett M, Wu T, Inaba A, Azuma R, Mizusawa H. Relationship and factor structure in multisystem neurodegeneration in Parkinson's disease.
Acta Neurol Scand: DOI: 10.1111/ane.12273.

Objectives – Parkinson's disease (PD) is a multisystem neurodegenerative disease. We aimed to identify the relationship and factor structure among its different features. *Materials & methods* – Motor, olfactory and cognitive function, and cardiac sympathetic denervation were evaluated in 125 patients with PD using the Unified Parkinson's Disease Rating Scale (UPDRS) part III score, odor stick identification test for the Japanese (OSIT-J), Mini-Mental State Examination (MMSE), and [^{123}I] meta-iodobenzylguanidine (MIBG) cardiac scintigraphy (heart-to-mediastinum (H/M) ratio). Pearson's correlation and multiple regression analysis were used to evaluate the association among the four measures with age, gender, and disease duration as the covariates. Exploratory factor analysis was used to identify the underlying factor structure among the measures and covariates. *Results* – Pearson's correlation and multiple regression analysis showed correlations between OSIT-J score and MIBG H/M ratio, OSIT-J and MMSE scores, UPDRS part III score and MIBG H/M ratio, UPDRS part III score and disease duration, and MMSE score and age. Factor analysis identified three factors: (i) age and MMSE score; (ii) MIBG H/M ratio and OSIT-J score; and (iii) UPDRS part III score and disease duration. *Conclusions* – Our results suggest that aging, PD-related pathogenesis, and disease duration underlie the multisystem neurodegeneration present in PD. Moreover, age and disease duration are the major risk factors for cognitive impairment and motor symptoms, respectively. Olfactory impairment and cardiac sympathetic denervation are strongly associated in PD.

T. Hattori[1,2,3], S. Orimo[2], M. Hallett[3], T. Wu[4], A. Inaba[2], R. Azuma[2], H. Mizusawa[1]

[1]Department of Neurology and Neurological Sciences, Graduate School, Tokyo Medical and Dental University, Tokyo, Japan; [2]Department of Neurology, Kanto Central Hospital, Tokyo, Japan; [3]Human Motor Control Section, National Institute of Neurological Disorders and Stroke, National Institutes of Health, Bethesda, MD, USA; [4]Clinical Neurosciences Program, National Institute of Neurological Disorders and Stroke, National Institutes of Health, Bethesda, MD, USA

Key words: Parkinson's disease; cardiac sympathetic degeneration; olfactory impairment; cognitive impairment; relationship; factor analysis

T. Hattori, Department of Neurology and Neurological Sciences, Graduate School, Tokyo Medical and Dental University, 1-5-45 Yushima, Bunkyo-ku, Tokyo 113-8519, Japan
Tel.: +81 3 5803 5234
Fax: +81 3 5803 0169
e-mail: takaaki-hattori@umin.ac.jp

Accepted for publication June 9, 2014

Introduction

PD is a multisystem neurodegenerative disease. The presence of Lewy bodies is the pathological hallmark of PD; they progressively accumulate in neurons and neurites of multiple neurotransmitter systems (1, 2). Although some studies reported a relationship among different features of patients with PD (3–9), there are no previous studies which systematically explored such relationships.

We focused on motor, cognitive, and olfactory functions, and cardiac sympathetic denervation in patients with PD. As neurodegeneration is a multifactorial process, confounding factors should be considered as covariates to assess relationships. PD commonly develops in an older population and age is known to be a risk factor (10, 11). Male gender is also a risk factor for developing PD (10, 11). PD is a neurodegenerative disorder and its features progress over time. Thus, we considered age, gender and disease duration as covariates.

We hypothesized that some of the clinical and laboratory measures and covariates are correlated, reflecting the underlying pathophysiology. We used Pearson's correlation and multiple regression analysis to prove the relationships. We also used exploratory factor analysis, which

is based on the assumption that there are unobserved latent variables accounting for the correlations among observed variables, to identify the underlying factor structure in the relationships.

This study aimed to identify the relationships and factor structure in multisystem neurodegeneration in PD by using clinical and laboratory measures and covariates for a large cohort of patients.

Materials and methods

Patients

We performed a retrospective chart review for 176 patients with PD who visited Kanto Central Hospital, a community hospital in Tokyo, Japan from 2008 to 2012. All examinations were performed for clinical purposes. All data were extracted from the hospital database.

Inclusion criteria were subjects who had an established diagnosis of PD according to the clinical diagnostic criteria of the United Kingdom Parkinson's Disease Society Brain Bank (12) and responded symptomatically to dopaminergic therapy.

Exclusion criteria were subjects with moderate or severe dementia, which was defined as having a Clinical Dementia Rating (CDR) ≥2 because they could not cooperate appropriately with the testing. Subjects who had severe diabetes mellitus or a past medical history of ischemic heart disease and/or thoracic surgery were also excluded. Subjects who were not evaluated for motor, olfactory, and cognitive function and cardiac sympathetic denervation within a 6-month interval were also ineligible.

Patients were evaluated with general and neurological examinations and the Mini-Mental State Examination (MMSE). CDR was scored with a semi-structured interview for patients and caregivers by neurologists (T.H., S.O., and R.A.). Olfactory function and cardiac sympathetic denervation were assessed using the odor stick identification test for the Japanese (OSIT-J) and ^{123}I-MIBG cardiac scintigraphy, respectively. Levodopa equivalent dose (LED) was calculated according to a previous study (13). Patients were classified by Hoehn-Yahr (HY) stage, and evaluated using the Unified Parkinson's Disease Rating Scale (UPDRS) by neurologists.

Based on the inclusion and exclusion criteria, 125 patients were included in the analysis, and 51 patients were excluded because their data were not evaluated within a 6-month interval.

This study was approved by the Institutional Review Board of Kanto Central Hospital, Japan. As this is a retrospective observational cohort study and extracted data were de-identified, written informed consent was waived.

Olfactory assessment

Olfactory function was assessed by OSIT-J (Daiichi Yakuhin Sangyo Co., Ltd., Tokyo, Japan). OSIT-J was described in detail in a previous study (4). In brief, we tested 12 different odorants familiar to the Japanese population: India ink, wood, perfume, menthol, Japanese orange, curry, gas for cooking, rose, Japanese cypress (hinoki), condensed milk, socks smelling of sweat, and roasted garlic. A subject was given six alternatives: four odor names, including one correct name, "not detected," and "unknown." The total number of correct answers for the 12 odorants constituted the OSIT-J score.

^{123}I-MIBG cardiac scintigraphy

Subjects were given an intravenous injection of 111 MBq ^{123}I-MIBG (FUJIFILM RI Pharma Co., Ltd., Tokyo, Japan). Chest images were obtained after 15 min for the early phase, and 3 h for the late phase, using a gamma camera (e.cam Signature, SIEMENS, Munich and Berlin, Germany). The relative organ uptake of ^{123}I-MIBG was determined by region-of-interest (ROI) analysis in the anterior planar view. The ratio of the average pixel count in the heart (H) to that in the mediastinum (M) (H/M ratio), and the washout ratio were calculated. The MIBG late phase H/M ratio (MIBG H/M ratio) was used as a marker of cardiac sympathetic denervation.

Statistical analysis

The assumption of normality was evaluated based on the residuals using the Shapiro–Wilk test. Box–Cox transformation was applied to the variables which did not meet the assumption. Thus, an inverse transformation was used for the MIBG H/M ratio and square-root transformation for the UPDRS part III score.

In the simple linear correlation analysis, Pearson's correlation coefficient determined the linear correlation between two continuous variables. Point biserial correlation coefficient determined associations between gender (categorical variable) and the other (continuous) variables.

In the multiple linear regression analysis, stepwise regression analysis was applied to explore the association among the seven clinical and laboratory measures and covariates. Here, MMSE,

UPDRS part III, OSIT-J score, and MIBG H/M ratio were treated as dependent and independent variables, while age, gender, and disease duration were the covariate variables. The significance level of 0.1 was used for model selection. Multi-co-linearity among independent variables was evaluated using the variance inflation factor (VIF). $P < 0.05$ was reported as statistically significant.

To identify the underlying factor structure, exploratory factor analysis was applied for the six clinical and laboratory measures and covariates. Principal component analysis was used to extract factors, followed by Varimax rotation and Kaiser Normalization. The number of factors was determined by interpretability. The absolute factor loading value of ≥0.60 was defined as a variable's large contribution to a factor. Absolute loading value <0.45, but ≥0.25 was defined as the intermediate contribution.

Statistical analysis was performed with the Scientific Package for Social Sciences version 20 (SPSS 20) (Armonk, NY, USA) and Statistical Analysis Software (SAS) (Cary, NC, USA).

Results

Patients' clinical and laboratory data are described in Table 1.

Pearson's correlation coefficients between measures and covariates are shown in Table 2. Gender was associated with OSIT-J score (mean 4.2 for men and 5.4 for women) and MMSE score (mean 25.9 for men and 27.4 for women).

Table 1 Demographic and clinical data of 125 patients with Parkinson's disease

Characteristics	Mean	SD
Age	72.9	8.4
Gender: M/F	57/68	–
Disease duration (months)	49.3	44.3
Hoehn-Yahr stage	1.8	0.4
Levodopa equivalent dose	183.5	256.2
MMSE score	26.7	2.9
OSIT-J score [8.2 (2.4)]	4.8	2.8
MIBG early phase H/M ratio [2.32 (0.33)]	1.81	0.43
MIBG late phase H/M ratio [2.35 (0.36)]	1.61	0.47
MIBG washout rate (%) [18.4 (9.0)]	29.0	8.9
UPDRS part I score	2.0	1.7
UPDRS part II score	10.0	5.4
UPDRS part III score	22.0	11.9
UPDRS part IV score	1.6	2.0

SD, standard deviation; UPDRS, Unified Parkinson's Disease Rating Scale; MMSE, Mini-Mental State Examination; OSIT-J, the odor stick identification test for the Japanese; MIBG, [^{123}I] *meta*-iodobenzylguanidine; H/M, heart/mediastinum.
Normal range of OSIT-J score, MIBG H/M ratio and MIBG washout rate are described by [mean (SD)].

Table 2 Pearson's (or point biserial) correlation coefficients

	OSIT-J score	MIBG late phase H/M ratio[a]	MMSE score	UPDRS part III score[b]
Pearson's correlation coefficient				
OSIT-J score	–	0.407***	0.336***	−0.300***
MIBG late phase H/M ratio[a]	0.407***	–	NS	−0.334***
MMSE score	0.336***	NS	–	−0.279**
UPDRS part III score[b]	−0.300***	−0.334***	−0.279**	–
Age	−0.259**	NS	−0.432***	0.336***
Disease duration	NS	−0.263**	NS	0.361***
Point biserial correlation coefficient				
Gender	−0.223*	NS	−0.264**	NS

n, number; OSIT-J, the odor stick identification test for the Japanese; MIBG, [^{123}I] *meta*-iodobenzylguanidine; H/M, heart/mediastinum; MMSE, Mini-Mental State Examination; UPDRS, Unified Parkinson's Disease Rating Scale.
[a]Inverse transformed.
[b]Square-root transformed.
NS: $P > 0.05$.
*$P < 0.05$.
**$P < 0.01$.
***$P < 0.001$.

The results of multiple regression analyses are summarized in Table 3. All variables included in the final models had VIF <2. Scatter plots for clinical and laboratory measures and covariates which were correlated in the multiple regression analysis are shown in Fig. 1.

Factor analysis was applied for the six clinical and laboratory measures and covariates, OSIT-J, MMSE, UPDRS part III score, MIBG H/M ratio, age, and disease duration. For these variables, Kaiser's MSA (measures of sampling adequacy) values were >0.62 (>0.5 is acceptable for factor analysis). The factor loadings are listed in Table 4. Factor analysis extracted three factors, which accounted for 62.6% of the total variance, from the six variables. For factor 1, MMSE score and age had high loadings while the OSIT-J score and UPDRS part III score had intermediate loadings. For factor 2, the MIBG H/M ratio and OSIT-J score had high loadings while UPDRS part III score had intermediate loading. For factor 3, UPDRS part III score and disease duration had high loadings while the MIBG H/M ratio had intermediate loading.

Discussion

To our knowledge, this is the first study to identify multiple relationships among motor, olfactory, and cognitive function and cardiac sympathetic denervation using Pearson's correlation and multiple regression analyses. We also identified three underlying factors in the relationships using factor analysis.

Table 3 Multiple regression analysis

	Dependent variable			
	OSIT-J score	MIBG late phase H/M ratio[a]	MMSE score	UPDRS part III score[b]
Independent variable	Squared type II semipartial correlation			
OSIT-J score		0.103***	0.035*	–
MIBG late phase H/M ratio[a]	0.142***		–	0.061**
MMSE score	0.089***	–		–
UPDRS part III score[b]	–	0.050**	–	
Age	–	–	0.126***	0.085***
Gender	–	–	0.036*	–
Disease duration	–	–	–	0.060**
R^2 for the model including all significant variables	0.255	0.215	0.276	0.276

n, number; OSIT-J, the odor stick identification test for the Japanese; MIBG, [^{123}I] *meta*-iodobenzylguanidine; H/M, heart/mediastinum; MMSE, Mini-Mental State Examination; UPDRS, Unified Parkinson's Disease Rating Scale.

[a]Inverse transformed.

[b]Square-root transformed.

'–' = Dropped from the model with $P > 0.1$.

*$P < 0.05$.

**$P < 0.01$.

***$P < 0.001$.

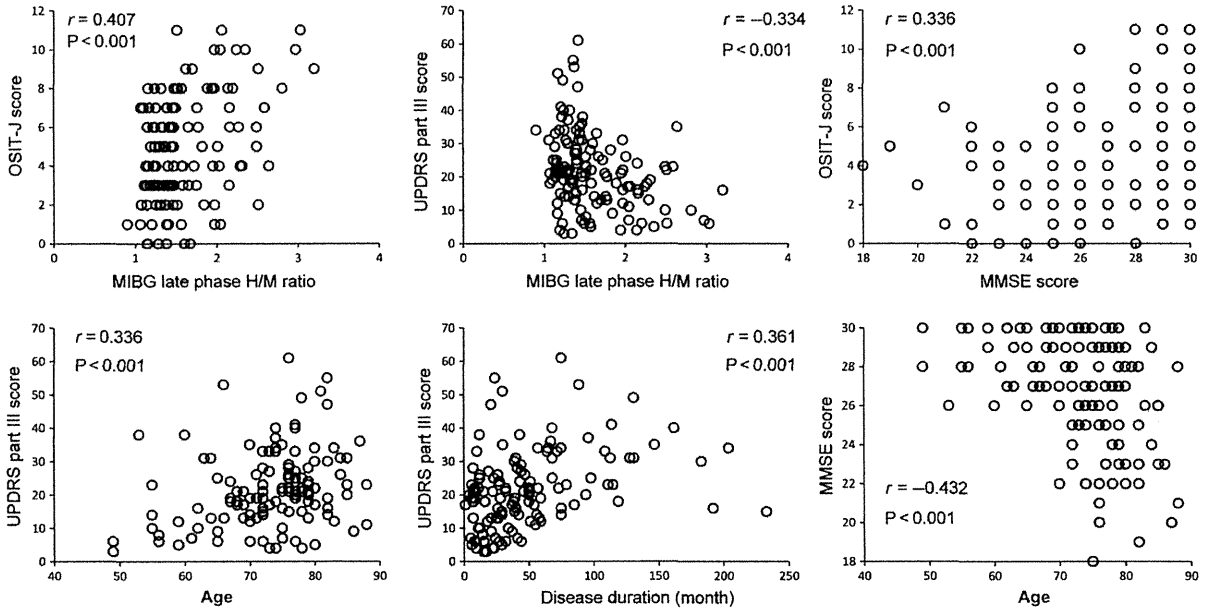

Figure 1. Scatter plots for clinical and laboratory measures and covariates which were correlated in a multiple regression analysis. OSIT-J, the Odor Stick Identification Test for the Japanese; MIBG, [123I] metaiodobenzylguanidine; H/M, heart/mediastinum; UPDRS, Unified Parkinson's Disease Rating Scale; MMSE, Mini-Mental State Examination. Pearson's correlation coefficient (r) and p value are calculated by Pearson correlation; MIBG late phase H/M ratio and UPDRS part III score are inverse transformed and square-root transformed, respectively. 90x48mm (300 x 300 DPI).

For factor 1, age and MMSE score had high loading while OSIT-J score and UPDRS part III score had intermediate loading. In the multiple regression analysis, age was correlated with MMSE, OSIT-J, and UPDRS part III score. Thus, we consider that factor 1 represents the aging effect on the clinical features of patients with PD. In other words, aging is the risk factor for cognitive function followed by smell and motor function. This finding is consistent with previous studies indicating that advanced age is a risk factor for developing PD (10, 11) and dementia in patients with PD (14, 15).

For factor 2, the MIBG H/M ratio and OSIT-J score had high loading, and UPDRS part III score had intermediate loading. The OSIT-J score

Table 4 Factor analysis of clinical and laboratory measures and covariates

Variable interpretation of factor	Factor 1 aging	Factor 2 PD-related pathogenesis	Factor 3 disease duration	Final communality estimate
Age	**0.826**	0.032	0.198	0.72
MMSE score	**−0.805**	0.194	0.008	0.69
MIBG late phase H/M ratio[a]	0.119	**0.828**	−0.299	0.79
OSIT-J score	−0.358	**0.790**	0.003	0.75
Disease duration	−0.013	−0.068	**0.893**	0.80
UPDRS part III score[b]	0.369	−0.277	**0.649**	0.63
Variance explained by each factor	1.61	1.43	1.35	4.38
	22.3%	20.4%	19.2%	62.6%

MMSE, Mini-Mental State Examination; MIBG, [^{123}I] *meta*-iodobenzylguanidine; H/M, heart/mediastinum; OSIT-J, the odor stick identification test for the Japanese; UPDRS, Unified Parkinson's Disease Rating Scale.
The high loading (larger than 0.60 by absolute value) in each factor is shown in bold and intermediate loading (larger than 0.25 and <0.60 by absolute value) is underlined.
[a]Inverse transformed.
[b]Square-root transformed.

and MIBG H/M ratio were correlated in the multiple regression analysis. While the exact pathophysiology of olfactory impairment remains to be elucidated, the broad olfactory-related areas, including the olfactory bulb, primary olfactory cortex, amygdala, hippocampus and orbitofrontal cortex, are susceptible to Lewy pathology. These structures are thought to be the neural substrates for olfactory impairment (16–19). Cardiac sympathetic nerves are also susceptible to Lewy pathology in PD. It is known that a decreased MIBG H/M ratio indicates the presence of degenerated noradrenergic cardiac sympathetic fibers due to Lewy body pathology (20). Both olfactory bulb and cardiac sympathetic nerves are supposed to have Lewy pathology in the very early phase of PD, even preceding the onset of motor symptoms (19–21). Thus, we consider that factor 2 represents the effect of PD-related pathogenesis, particularly resulting in Lewy pathology in the olfactory-related areas and cardiac sympathetic nerves in the very early stage of PD. On the other hand, while motor and cognitive functions are also supposed to be related to Lewy pathology, their loadings were intermediate (−0.277) and low (0.194) in factor 2, respectively. Although the reason for this is not clear, it might be because motor and cognitive functions are also strongly influenced by disease duration (factor 3) and age (factor 1), respectively, resulting in relatively lighter loading in factor 2.

For factor 3, the UPDRS part III score and disease duration had high loading and the MIBG H/M ratio had intermediate loading. Disease duration was correlated with motor function in multiple regression analyses and with the MIBG H/M ratio in only the Pearson's correlation analysis. Thus, we consider that factor 3 represents the effect of disease duration for motor function followed by the MIBG H/M ratio.

Taken together, we determined that aging, PD-related pathogenesis, and disease duration underlie the multisystem neurodegeneration in PD. It is interesting to note that motor symptoms and non-motor features (cognitive and olfactory impairment and cardiac sympathetic denervation) were loaded in separate factors, suggesting that a somewhat different pathophysiology accelerates the motor symptoms and non-motor features of PD. Our results suggest that age is the major risk factor for cognitive impairment in PD (factor 1). To date, various pathogenetic mechanisms (2, 22), for example cortical Lewy bodies (23, 24), Alzheimer's disease-type pathologies (25) and white matter damage (26) were suggested as neural correlates of cognitive impairment in PD. It is also known that multiple neurotransmitter systems, for example acetylcholine, dopamine, serotonin, and noradrenaline, could be targeted in PD, and their degeneration may underlie the different phenotypes of cognitive deficits (27, 28). We speculate that aging may interact with the PD-related pathogenesis in the cognitive-related areas, accelerating the degeneration of certain neurotransmitter systems, resulting in cognitive deficits. On the other hand, our study also showed that disease duration is the main risk factor for motor symptoms (factor 3). This is consistent with the natural history of PD as a progressive neurodegenerative disease, that is motor symptoms progress throughout the course of the disease. Furthermore, our results showed a strong association between olfactory impairment and cardiac sympathetic denervation (factor 2). A similar association was also reported in several previous studies (3–5). While ^{123}I-MIBG cardiac scintigraphy specifically evaluates noradrenergic nerves, olfactory impairment is supposed to reflect impaired multiple neurotransmitter systems such as acetylcholine, serotonin, dopamine, and noradrenaline (29). We speculate that the two systems share a common pathogenesis which might be affected even during the very early phase of PD. For example, they may share the catecholamine (i.e., dopamine and noradrenaline) systems, which might have similar biochemical processes such as aldehyde formation (30), resulting in Lewy pathology and underlying their strong association. The exact pathological and

biochemical correlates should be investigated in future studies.

In the multiple regression analysis, OSIT-J and MMSE scores were also correlated. To date, this relationship is somewhat controversial. Some studies did not find the relationship (4, 5), whereas Baba et al. (6) reported a weak correlation between OSIT-J score and MMSE score and Bohnen et al. (31) found a relationship between odor identification score and cognitive measures of episodic verbal learning. We enrolled various patients with PD ranging from those who were cognitively normal to those who had mild dementia, despite the fact that most previous studies evaluated only PD patients without dementia. Thus, we found the association because we had a greater number of subjects with wide-ranging clinical variability. On the other hand, the neural basis of this correlation is still obscure. Olfactory perception is known to require semantic processing (32). Hudry et al. (33) pointed out that olfactory impairment in patients with PD is partly due to deficiencies in perceptual and semantic olfactory processes. Moreover, it was also reported that olfactory impairment is related to cholinergic denervation of the limbic archicortex (31); severe hyposmia predicts future development of dementia in these patients (34). Thus, olfactory and cognitive function may share the same anatomy, impairment in the same neurotransmitter systems and/or the same functional systems such as semantic processing. Further study is needed to identify the neural correlates of this association.

In a multiple regression analysis, UPDRS part III score and the MIBG H/M ratio were negatively correlated. Kim et al. (7) reported that the MIBG H/M ratio is related to severity of midline motor symptoms in patients with PD, but not to HY stage nor UPDRS part III score. Spiegel et al. (8) reported that the MIBG H/M ratio correlated with the severity of hypokinesia and rigidity, but not with the severity of a resting or postural tremor in patients with PD. While we used only the total score of UPDRS part III score, certain components of the motor symptoms might specifically correlate with the MIBG H/M ratio, supporting the correlation that we found. Future study is needed to clarify the pathophysiology of this association.

Braak et al. (19) proposed the progression patterns of Lewy pathology in PD. In summary, Lewy pathology is found in the anterior olfactory structures in stages 1–2, progresses to the substantia nigra and other nuclei of the basal mid- and forebrain, and motor and cognitive symptoms manifest in stages 3–4 (23). Lewy pathology further extends to the neocortex, and motor, and cognitive function worsens in stages 5–6. As discussed above, OSIT-J and MMSE score reflect the synergistic cortical functions of olfactory- and cognitive-related areas. Thus, the association between OSIT-J and MMSE score may suggest parallel neurodegeneration due to Lewy pathology in the olfactory- and cognitive-related areas during stages 3–6. On the other hand, pathology in the cardiac sympathetic nerves is not defined in Braak staging (19). Based on the association between MIBG H/M ratio and OSIT-J score or HY/UPDRS part 3 score, we speculate that cardiac sympathetic nerves also degenerate in parallel to Lewy pathology in brain. Thus, the MIBG H/M ratio could be used as a biomarker of accumulated Lewy pathology in the brains of patients with PD. The correspondence between Braak staging and olfactory impairment/cardiac sympathetic denervation should be investigated in a future study.

Some limitations of the present study should be addressed. First, this is both cross-sectional and retrospective in design and did not allow us to observe features longitudinally. A longitudinal study is needed to prove the associated degeneration directly. Second, this study did not include data on several key non-motor symptoms such as psychiatric symptoms, hallucination, mood disorders, and sleep problems. A future prospective study assessing the various features of PD is needed to thoroughly investigate the relationships. Third, this study design does not identify the underlying pathogenesis behind the observed multisystem degeneration. Various levels of future studies, such as genetic, molecular, receptor (35), neurotransmitter and biochemical process (30), are needed to elucidate this point.

In conclusion, this study suggests that three parallel processes, aging, PD-related pathogenesis and disease duration underlie the multisystem neurodegeneration in PD. Our study also revealed that age and disease duration are the main risk factors for cognitive impairment and motor function, respectively, while cardiac sympathetic denervation and olfactory impairment are strongly associated. The data taken together support the current idea of PD as a progressive neurodegenerative disease. Age plays a significant role in the disease process and interacts with PD-related pathogenesis to accelerate PD symptoms (15).

Acknowledgements

We would like to thank Devera G. Schoenberg, M.Sc. Editor, Office of the Clinical Director, National Institute of Neurological Disorders and Stroke, National Institutes of Health, and

Cindy Clark, NIH Library Editing Service, for reviewing the manuscript. We would also like to thank Yoko Fukai, department of neurology, Kanto Central Hospital, for data collection.

Sources of funding

This study had no funding. Dr. Hallett, and currently Dr. Hattori, are supported by the NINDS Intramural Program.

Conflict of interest

The authors have no conflict of interest to report.

References

1. Langston JW. The Parkinson's complex: parkinsonism is just the tip of the iceberg. Ann Neurol 2006;**59**:591–6.
2. Jellinger KA. Neuropathology of sporadic Parkinson's disease: evaluation and changes of concepts. Mov Disord 2012;**27**:8–30.
3. Goldstein DS, Sewell L, Holmes C. Association of anosmia with autonomic failure in Parkinson disease. Neurology 2010;**74**:245–51.
4. Iijima M, Osawa M, Momose M et al. Cardiac sympathetic degeneration correlates with olfactory function in Parkinson's disease. Mov Disord 2010;**25**:1143–9.
5. Oka H, Toyoda C, Yogo M, Mochio S. Olfactory dysfunction and cardiovascular dysautonomia in Parkinson's disease. J Neurol 2010;**257**:969–76.
6. Baba T, Takeda A, Kikuchi A et al. Association of olfactory dysfunction and brain. Metabolism in Parkinson's disease. Mov Disord 2011;**26**:621–8.
7. Kim JS, Lee KS, Song IU et al. Cardiac sympathetic denervation is correlated with Parkinsonian midline motor symptoms. J Neurol Sci 2008;**270**:122–6.
8. Spiegel J, Hellwig D, Farmakis G et al. Myocardial sympathetic degeneration correlates with clinical phenotype of Parkinson's disease. Mov Disord 2007;**22**:1004–8.
9. Pfeiffer HC, Lokkegaard A, Zoetmulder M, Friberg L, Werdelin L. Cognitive impairment in early-stage non-demented Parkinson's disease patients. Acta Neurol Scand 2014;**129**:307–18.
10. Kieburtz K, Wunderle KB. Parkinson's disease: evidence for environmental risk factors. Mov Disord 2013;**28**:8–13.
11. De Lau LM, Breteler MM. Epidemiology of Parkinson's disease. Lancet Neurol 2006;**5**:525–35.
12. Hughes AJ, Daniel SE, Kilford L, Lees AJ. Accuracy of clinical diagnosis of idiopathic Parkinson's disease: a clinico-pathological study of 100 cases. J Neurol Neurosurg Psychiatry 1992;**55**:181–4.
13. Tomlinson CL, Stowe R, Patel S, Rick C, Gray R, Clarke CE. Systematic review of levodopa dose equivalency reporting in Parkinson's disease. Mov Disord 2010; **25**:2649–53.
14. Hobson P, Meara J. Risk and incidence of dementia in a cohort of older subjects with Parkinson's disease in the United Kingdom. Mov Disord 2004;**19**:1043–9.
15. Levy G. The relationship of Parkinson disease with aging. Arch Neurol 2007;**64**:1242–6.
16. Silveira-Moriyama L, Holton JL, Kingsbury A et al. Regional differences in the severity of Lewy body pathology across the olfactory cortex. Neurosci Lett 2009; **453**:77–80.
17. Hubbard PS, Esiri MM, Reading M, Mcshane R, Nagy Z. Alpha-synuclein pathology in the olfactory pathways of dementia patients. J Anat 2007;**211**:117–24.
18. Ubeda-Banon I, Saiz-Sanchez D, De La Rosa-Prieto C, Argandona-Palacios L, Garcia-Munozguren S, Martinez-Marcos A. Alpha-Synucleinopathy in the human olfactory system in Parkinson's disease: involvement of calcium-binding protein- and substance P-positive cells. Acta Neuropathol 2010;**119**:723–35.
19. Braak H, Del Tredici K, Rub U, De Vos RA, Jansen Steur EN, Braak E. Staging of brain pathology related to sporadic Parkinson's disease. Neurobiol Aging 2003; **24**:197–211.
20. Orimo S, Takahashi A, Uchihara T et al. Degeneration of cardiac sympathetic nerve begins in the early disease process of Parkinson's disease. Brain Pathol 2007;**17**: 24–30.
21. Haehner A, Hummel T, Hummel C, Sommer U, Junghanns S, Reichmann H. Olfactory loss may be a first sign of idiopathic Parkinson's disease. Mov Disord 2007; **22**:839–42.
22. Irwin DJ, White MT, Toledo JB et al. Neuropathologic substrates of Parkinson disease dementia. Ann Neurol 2012;**72**:587–98.
23. Braak H, Rub U, Jansen Steur EN, Del Tredici K, De Vos RA. Cognitive status correlates with neuropathologic stage in Parkinson disease. Neurology 2005;**64**:1404–10.
24. Mattila PM, Rinne JO, Helenius H, Dickson DW, Roytta M. Alpha-synuclein-immunoreactive cortical Lewy bodies are associated with cognitive impairment in Parkinson's disease. Acta Neuropathol 2000;**100**:285–90.
25. Kalaitzakis ME, Pearce RK. The morbid anatomy of dementia in Parkinson's disease. Acta Neuropathol 2009; **118**:587–98.
26. Hattori T, Orimo S, Aoki S et al. Cognitive status correlates with white matter alteration in Parkinson's disease. Hum Brain Mapp 2012;**33**:727–39.
27. Kehagia AA, Barker RA, Robbins TW. Neuropsychological and clinical heterogeneity of cognitive impairment and dementia in patients with Parkinson's disease. Lancet Neurol 2010;**9**:1200–13.
28. Shulman JM, De Jager PL, Feany MB. Parkinson's disease: genetics and pathogenesis. Annu Rev Pathol 2011;**6**:193–222.
29. Doty RL. Olfactory dysfunction in Parkinson disease. Nat Rev Neurol 2012;**8**:329–39.
30. Goldstein DS. Stress, allostatic load, catecholamines, and other neurotransmitters in neurodegenerative diseases. Cell Mol Neurobiol 2012;**32**:661–6.
31. Bohnen NI, Muller ML, Kotagal V et al. Olfactory dysfunction, central cholinergic integrity and cognitive impairment in Parkinson's disease. Brain 2010;**133**: 1747–54.
32. Royet JP, Plailly J. Lateralization of olfactory processes. Chem Senses 2004;**29**:731–45.
33. Hudry J, Thobois S, Broussolle E, Adeleine P, Royet JP. Evidence for deficiencies in perceptual and semantic olfactory processes in Parkinson's disease. Chem Senses 2003;**28**:537–43.
34. Baba T, Kikuchi A, Hirayama K et al. Severe olfactory dysfunction is a prodromal symptom of dementia associated with Parkinson's disease: a 3 year longitudinal study. Brain 2012;**135**:161–9.
35. Casetta I, Vincenzi F, Bencivelli D et al. A2A adenosine receptors and Parkinson's disease severity. Acta Neurol Scand 2014;**129**:276–81.

Citation: Molecular Therapy—Nucleic Acids (2015) 4, e220; doi:10.1038/mtna.2014.72

www.nature.com/mtna

Chimeric Antisense Oligonucleotide Conjugated to α-Tocopherol

Tomoko Nishina[1,2], Junna Numata[1], Kazutaka Nishina[1,2], Kie Yoshida-Tanaka[1,2], Keiko Nitta[1], Wenying Piao[1,2], Rintaro Iwata[2,3], Shingo Ito[4], Hiroya Kuwahara[1,2], Takeshi Wada[2,3], Hidehiro Mizusawa[1,5] and Takanori Yokota[1,2,5]

We developed an efficient system for delivering short interfering RNA (siRNA) to the liver by using α-tocopherol conjugation. The α-tocopherol–conjugated siRNA was effective and safe for RNA interference–mediated gene silencing *in vivo*. In contrast, when the 13-mer LNA (locked nucleic acid)-DNA gapmer antisense oligonucleotide (ASO) was directly conjugated with α-tocopherol it showed markedly reduced silencing activity in mouse liver. Here, therefore, we tried to extend the 5′-end of the ASO sequence by using 5′-α-tocopherol–conjugated 4- to 7-mers of unlocked nucleic acid (UNA) as a "second wing." Intravenous injection of mice with this α-tocopherol–conjugated chimeric ASO achieved more potent silencing than ASO alone in the liver, suggesting increased delivery of the ASO to the liver. Within the cells, the UNA wing was cleaved or degraded and α-tocopherol was released from the 13-mer gapmer ASO, resulting in activation of the gapmer. The α-tocopherol–conjugated chimeric ASO showed high efficacy, with hepatic tropism, and was effective and safe for gene silencing *in vivo*. We have thus identified a new, effective LNA-DNA gapmer structure in which drug delivery system (DDS) molecules are bound to ASO with UNA sequences.

Molecular Therapy—Nucleic Acids (2015) **4**, e220; doi:10.1038/mtna.2014.72; published online 13 January 2015
Subject Category: Nucleic acid chemistries Antisense oligonucleotides

Introduction

Antisense oligonucleotides (ASOs) and small interfering RNA (siRNA) are both recognized therapeutic agents for the silencing of specific genes at the posttranscriptional level.[1] Chemical modifications, particularly the use of locked nucleic acids (LNAs),[2–4] 2′-*O*-methoxyethyl (2′-*O*-MOE),[5,6] and constrained ethyl BNA (cEt),[7,8] markedly improve ASO binding affinity for the target mRNA, resulting in increased steric block efficiency. Currently, the mainstream of the ASO is gapmer ASOs.[1] Gapmer oligonucleotides, which contain two to five chemically modified nucleotides (LNA, 2′-*O*-MOE RNA, or cEt) as "wings" at each terminus flanking a central 5- to 10-base "gap" of DNA, enable cleavage of the target mRNA by RNase H, which recognizes DNA/RNA heteroduplexes.[9,10]

Recently, the FDA approved Kynamro (mipomersen sodium, Isis Pharmaceuticals, Carlsbad, CA) as a treatment for familial hypercholesterolemia.[11,12] Kynamro, a DNA 10-mer with 2′-*O*-MOE-modified-5-mers at both ends, targets *Apolipoprotein B* (*ApoB*). It has a strong target gene–silencing effect and greatly reduces serum low-density lipoprotein (LDL)-cholesterol in patients with familial hypercholesteremia. Since the approval of Kynamro, the higher binding affinity of LNAs has prompted the development of far shorter ASOs, which have been shown recently to increase the gene silencing effect, probably because of their increased intracellular availability.[13] Despite this progress in the design of new chemical modifications of oligonucleotides, methods that improve the potency of oligonucleotide drugs in animals are still highly desirable. The inadequate delivery and poor cellular uptake of oligonucleotides, coupled with their inability to efficiently access the target mRNA during intracellular trafficking,[14] are major impediments to *in vivo* silencing.[15]

The development of effective delivery systems for oligonucleotides is essential for their clinical application. Previously, we hypothesized that the best *in vivo* carrier for siRNA would be a molecule that the target cells need but cannot synthesize. Vitamins meet these requirements, and the least toxic, fat-soluble vitamin (even at high doses) is vitamin E.[16] Therefore, we directly conjugated α-tocopherol, a natural isomer of vitamin E, to siRNA and obtained a substantial reduction in the expression of an endogenous gene in mouse liver and brain.[17,18] In this study, we tried to use α-tocopherol (Toc) conjugation as a delivery system for ASO.

Results

Design of Toc-ASO targeting mouse *ApoB* mRNA

We used the 13-mer LNA/DNA gapmer that targets mouse *ApoB* mRNA (NM_009693) and has been described previously.[13] Toc was conjugated to several lengths of gapmers or chimeric ASOs. The structures of the α-tocopherol-bound ASO (Toc-ASOs) are shown in Figure 1. For example, the 20-mer Toc-ASO is an α-tocopherol–conjugated chimeric 20-mer, with a 7-mer "second wing" (Figure 1) of artificial nucleotides extending from the 5′-end of the original 13-mer ASO. The 7-mer second wing was composed of phosphodiester-bound unlocked nucleic acid (UNA) (Toc-20-mer ASO) or phosphorothioate-bound UNA (Toc-20-mer ASO PS). To estimate the effect of the artificial modification second wing, we

The first two authors contributed equally to this work.
[1]Department of Neurology and Neurological Science, Graduate School, Tokyo Medical and Dental University, Tokyo, Japan; [2]Core Research for Evolutional Science and Technology (CREST), Japan Science and Technology Agency (JST), Tokyo, Japan; [3]Faculty of Pharmaceutical Sciences, Tokyo University of Science, Chiba, Japan; [4]Department of Pharmaceutical Microbiology, Kumamoto University, Kumamoto, Japan; [5]The Center for Brain Integration Research, Tokyo Medical and Dental University, Tokyo, Japan. Correspondence: Takanori Yokota, Department of Neurology and Neurological Science, Graduate School, Tokyo Medical and Dental University, 1-5-45 Yushima, Bunkyo-ku, Tokyo 113–8519, Japan. E-mail: tak-yokota.nuro@tmd.ac.jp
Received 14 May 2014; accepted 26 November 2014; published online 13 January 2015. doi:10.1038/mtna.2014.72

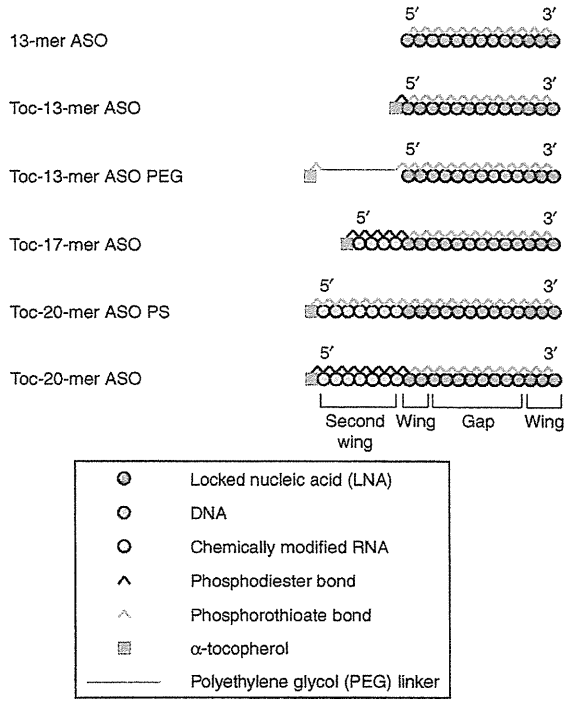

Figure 1 Design of several types of Toc-ASOs.

synthesized α-tocopherol-bound 17-mer ASO with second wing consisting of phosphodiester-bound 2′-Fluoro modified RNA (Toc-17-mer ASO F) and phosphodiester-bound 2′-*O*-methyl RNA (Toc-17-mer ASO OMe).

To estimate the length effect of the second wing, we designed several lengths of Toc-chimeric ASOs that contained phosphodiester-bound UNA, namely Toc-14-mer ASO, Toc-17-mer ASO, and Toc-23-mer ASO. To estimate α-tocopherol conjugation effect, we designed α-tocopherol–unconjugated ASOs with phosphodiester-bound UNA second wing: 14-mer ASO, 17-mer ASO, and 20-mer ASO.

The UV melting temperatures (T_m) of various Toc-ASOs are shown in Table 1. All of the Toc-ASOs had approximately the same T_m value, with the exception of Toc-17-mer ASO OMe and Toc-17-mer ASO F.

Table 1 Melting temperatures (T_m) of ASOs targeting mouse *Apolipoprotein B* (*ApoB*) mRNA

ASO	T_m (°C)
13-mer ASO	58.9
Toc-13-mer ASO	58.0
14-mer ASO	58.1
Toc-14-mer ASO	57.9
17-mer ASO	57.8
Toc-17-mer ASO	56.5
Toc-17-mer ASO F	71.4
Toc-17-mer ASO OMe	69.9
20-mer ASO	58.1
Toc-20-mer ASO	57.4
Toc-20-mer ASO PS	55.8
Toc-23-mer ASO	56.8

Efficacy of the Toc-ASOs

First, we made a nucleic acid Toc-13-mer ASO, in which the α-tocopherol was directly conjugated to the 13-mer ASO by a phosphodiester bond. Mice were injected with 0.75 mg/kg ASO and examined 3 days later. Quantitative reverse transcriptase polymerase chain reaction (RT-PCR) was performed using total RNA extracted from liver homogenates. We found that the Toc-13-mer ASO had no gene silencing effect (Figure 2a). Because conjugation of α-tocopherol interfered with the 13-mer ASO's gene silencing effect, we introduced a spacer between the 13-mer ASO and α-tocopherol. Because Toc-13-mer ASO PEG (α-tocopherol–conjugated to the 13-mer ASO via hexaethylene glycol) also had no effect, we then inserted additional nucleotides as a linker for spacing. Although Toc-20-mer ASO PS had no gene silencing effect (Figure 2a), Toc-17-mer and Toc-20-mer ASOs reduced target gene expression, especially Toc-17-mer ASO had significantly greater effect than that of the parent 13-mer ASO (Figure 2a).

Length effect of the second wing

Toc-13-mer (no second wing sequences) and Toc-14-mer ASO had no obvious effect, but Toc-17-mer and Toc-20-mer ASOs decreased the target gene expression. Importantly, these silencing effects were more potent than that of the 13-mer ASO (Figure 2b). To verify the advantage of α-tocopherol conjugation, the gene silencing effects of several length of ASOs with α-tocopherol conjugation or without α-tocopherol conjugation were evaluated. The ASOs without α-tocopherol did not have target gene silencing effect (Figure 2b). The knockdown effect was specific for the target molecule, as evidenced by the findings that the negative control of Toc-17-mer or Toc-20-mer ASOs targeting an unrelated gene did not affect the *ApoB* mRNA level (Figure 2a,b), and that *ApoB* targeting Toc-ASOs did not change the levels of the other endogenous mRNAs in the liver—for example, *glyceraldehyde-3-phosphate dehydrogenase* (*Gapdh*), *transthyretin* (*Ttr*), *superoxide dismutase 1* (*Sod1*), and *hypoxanthine guanine phosphoribosyltransferase* (*Hprt*) (Figure 2c).

Chemical modification of the second wing

The target gene silencing effects of Toc-17-mer ASO F and Toc-17-mer ASO OMe was markedly reduced in comparison with Toc-17-mer ASO which had UNA second wing (Figure 2a).

To evaluate the difference of mechanisms between effective Toc-ASO and noneffective one, northern blot analysis was performed on mouse liver at 72 hours after 0.75 mg/kg injection of Toc-ASOs. Toc-17-mer ASO OMe produced only one band corresponding to full length of Toc-17-mer ASO OMe itself, and the Toc-17-mer ASO produced a band corresponding to 13-mer ASO, which indicated that the 13-mer ASO was cleaved from Toc-17-mer ASO *in vivo* (Figure 2d). Additionally, Toc-17-mer ASO F produced two bands: the cleaved 13-mer and the full length of Toc-17-mer

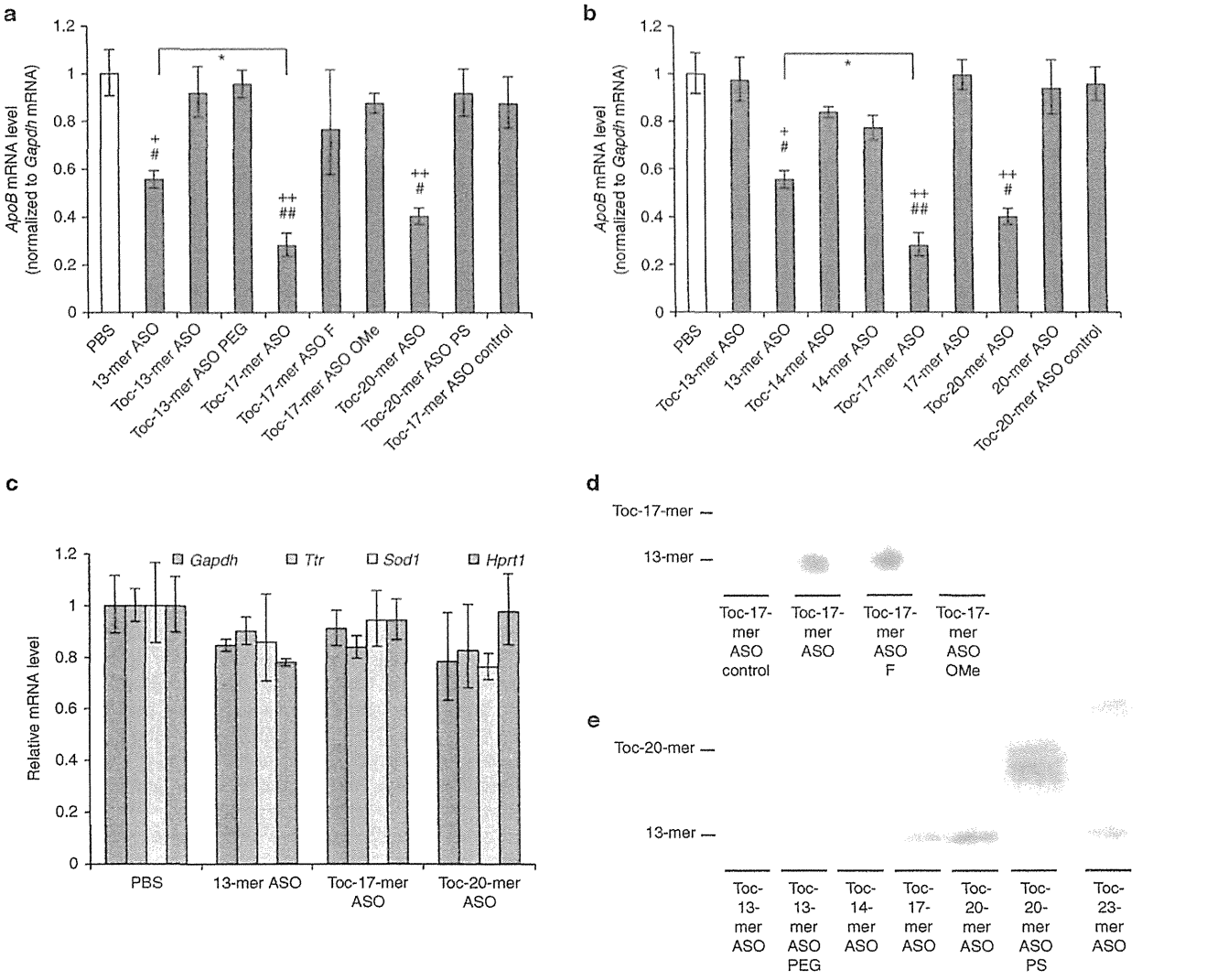

Figure 2 Gene-silencing effect of intravenous injection of Toc-ASO. (**a**) Quantitative RT-PCR analyses of *Apolipoprotein B* (*ApoB*) mRNA levels relative to *gapdh* mRNA levels in the liver 3 days after injection of 0.75 mg/kg α-tocopherol–conjugated ASOs. The data shown are relative to those from mice that received PBS alone and are presented as mean values ± SEM ($n = 3$, $^{+}P < 0.05$, $^{++}P < 0.01$ versus PBS, $^{\#}P < 0.05$, $^{\#\#}P < 0.01$, versus Toc-17-mer ASO control, and $^{*}P < 0.05$ Toc-17-mer ASO versus 13-mer ASO). (**b**) Quantitative RT-PCR analyses of *ApoB* mRNA levels (normalized to *gapdh* mRNA levels) in the liver 3 days after injection of 0.75 mg/kg ASOs bound to α-tocopherol by UNA second wings of various lengths or ASO without α-tocopherol. The data shown are relative to those from mice that received PBS alone and are presented as mean values ± SEM ($n = 3$, $^{+}P < 0.05$, $^{++}P < 0.01$ versus PBS, $^{\#}P < 0.05$, $^{\#\#}P < 0.01$ versus Toc-20-mer ASO control, and $^{*}P < 0.05$ between each groups). (**c**) Quantitative RT-PCR analyses of endogenous mRNAs (*Gapdh*, *Ttr*, *Sod1*, and *Hprt*) in the liver 3 days after injection of 0.75 mg/kg ASO, Toc-ASOs, or PBS alone. Data are relative to the total input RNA and are expressed as mean values ± SEM ($n = 3$). (**d**) Northern blot analysis to detect 13-mer gapmer sequences of Toc-ASO in the liver 3 days after injection of mice with 0.75 mg/kg Toc-ASO. (**e**) Northern blot analysis to detect 13-mer gapmer sequences of Toc-ASOs in the liver 3 days after injection of mice with 0.75 mg/kg Toc-ASOs of various lengths.

ASO F, it suggested that Toc-17-mer ASO F was thought to be less likely to be cleaved than Toc-17-mer ASO. In the liver samples from the 0.75 mg/kg Toc-ASO–injected mice on 72 hours after injection, the 13-mer band was clearly detected when mice were injected with the Toc-17-mer, Toc-20-mer, and Toc-23-mer ASOs (Figure 2e). On the other hand, samples from Toc-ASO–injected mouse liver in which Toc-ASOs had no silencing effect did not produce a 13-mer band (Figure 2e).

Dose dependency and time course of the Toc-ASOs effect

We derived dose-response curves from our quantitative RT-PCR results and then calculated the median effective dose (ED_{50})—that is, the dose of ASO that produced a 50% reduction in the target gene expression. We administered 0.75, 1.5, and 3 mg/kg of ASOs to mice and then sampled their livers (Figure 3a). We observed a dose dependent gene silencing effect in both 13-mer ASO and Toc-17-mer ASO-injected

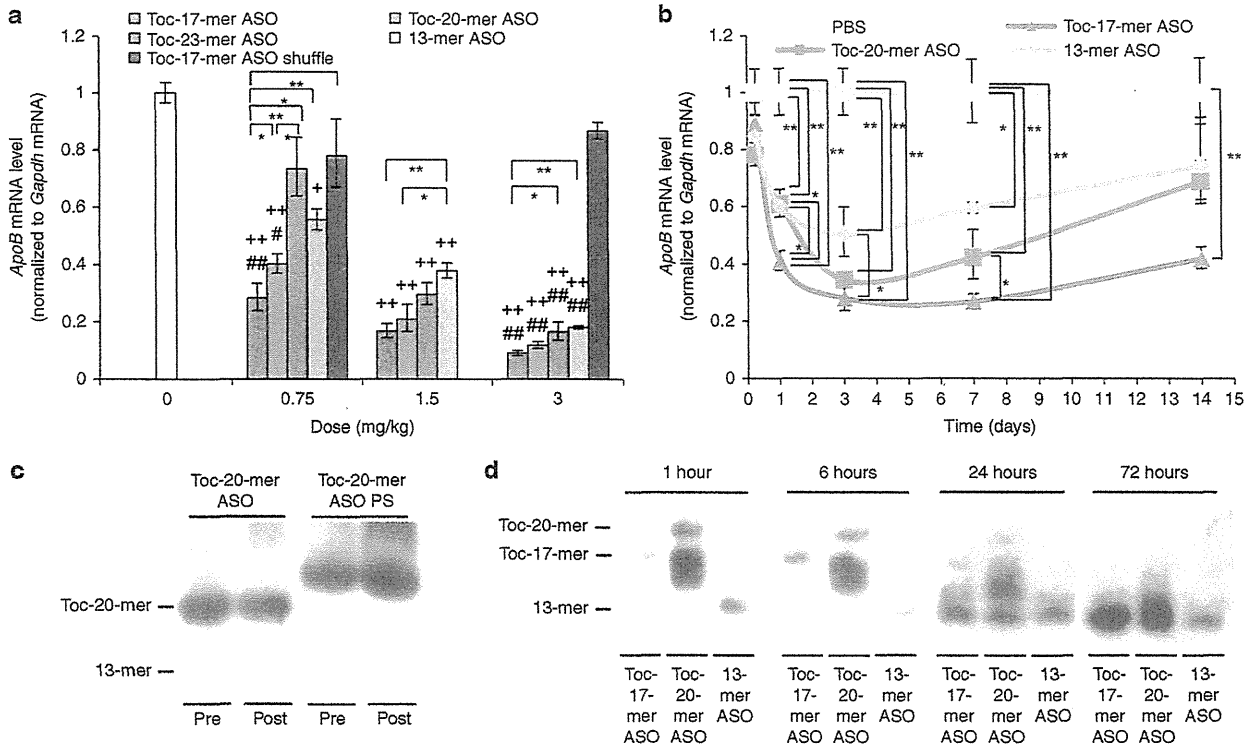

Figure 3 Dose-dependent reductions in mRNA levels and time course of gene silencing by intravenous injection of Toc-ASOs. (**a**) Dose-dependent reduction of gene by intravenous injection of Toc-ASOs. Quantitative RT-PCR analyses of *Apolipoprotein B* (*ApoB*) mRNA levels relative to *gapdh* mRNA levels in 3 days after injection of 0.75, 1.5 or 3 mg/kg Toc-ASOs. The data shown are relative to those from mice that received PBS alone and are presented as mean values ± SEM ($n = 3$, $^{+}P < 0.05$, $^{++}P < 0.01$ versus PBS, $^{\#}P < 0.05$, $^{\#\#}P < 0.01$ versus Toc-17-mer ASO shuffle, and $^{*}P < 0.05$, $^{**}P < 0.01$ between each groups). (**b**) Duration of gene silencing by intravenous injection of Toc-ASOs. Quantitative RT-PCR analyses of *Apolipoprotein B* (*ApoB*) mRNA levels relative to *gapdh* mRNA levels in the liver 6 hours, 1, 3, 7, and 14 after injection of 0.75 mg/kg Toc-ASOs. The data shown are relative to those from mice that received PBS alone and are presented as mean values ± SEM ($n = 3$, $^{*}P < 0.05$, $^{**}P < 0.01$). (**c**) The stability of Toc-ASOs. Toc-20-mer ASO and Toc-20-mer ASO PS were incubated in mouse serum with protease inhibitor for 24 hours at 37 °C. The samples were estimated by northern blot analysis to detect 13-mer gapmer sequences of Toc-ASO. (**d**) Northern blot analysis to detect 13-mer gapmer sequences of Toc-ASO in the liver 1 hour to 3 days after injection of mice with 0.75 mg/kg of each ASOs.

mice. The respective ED_{50} values for Toc-17-mer ASO, Toc-20-mer ASO, Toc-23-mer ASO, and 13-mer ASO were 24, 60, 145, and 216 nmol/kg. This indicating that Toc-17-mer ASO, Toc-20-mer and Toc-23-mer ASO were more efficacious than 13-mer ASO. We then examined the time courses of their effects. Mice were injected with 0.75 mg/kg of these α-tocopherol–conjugated ASOs, and their livers were collected from 6 hours to 14 days after injection. The gene silencing effects of 13-mer ASO, Toc-17-mer ASO, and Toc-20-mer ASO were observed 1 day after injection. The Toc-17-mer and Toc-20-mer ASOs showed significantly stronger than 13-mer ASO gene silencing effects from days 3 to 14 and days 3 to 7, respectively (Figure 3b).

Next, in order to know whether the Toc-ASOs were cleaved before or after reaching the liver, stability studies were performed on Toc-20-mer ASO and Toc-20-mer ASO PS. Both of the Toc-ASOs were incubated in mouse serum with protease inhibitor for 24 hours at 37 °C. In northern blot analysis to detect ASO, both Toc-20-mer-ASO and Toc-20-mer-ASO PS were stable 24 hours after incubation with mice serum (Figure 3c). We then examined *in vivo* analysis and performed northern blot analysis to detect ASO. Mice were injected with 0.75 mg/kg of Toc-ASOs, and their livers were collected at 1, 6, 24, and 72 hours after injection. The several bands including the full length of Toc-17-mer and Toc-20-mer ASOs were observed at 24 hours or earlier time point of after injection, and only 13-mer ASOs were detected at 72 hours after injection of Toc-17-mer and Toc-20-mer ASOs (Figure 3d). These results suggested that Toc-17-mer ASO and Toc-20-mer ASOs reached the liver with full length, and then were cleaved to 13-mer ASO.

In vivo pharmacokinetics

To determine whether Toc-ASOs was predominantly distributed to liver in mouse after intravenous injection, the *in vivo* tissue accumulation of Toc-ASOs was examined for 6 hours after intravenous injection of Toc-ASOs labeled with Alexa Fluor 647 at the 3′-ends. The accumulation of Toc-ASOs in the mouse liver was ~3.5-fold higher than that of α-tocopherol–unconjugated ASOs while the accumulation of Toc-ASOs in the mouse kidney was approximately six-fold lower than that of α-tocopherol–unconjugated ASOs

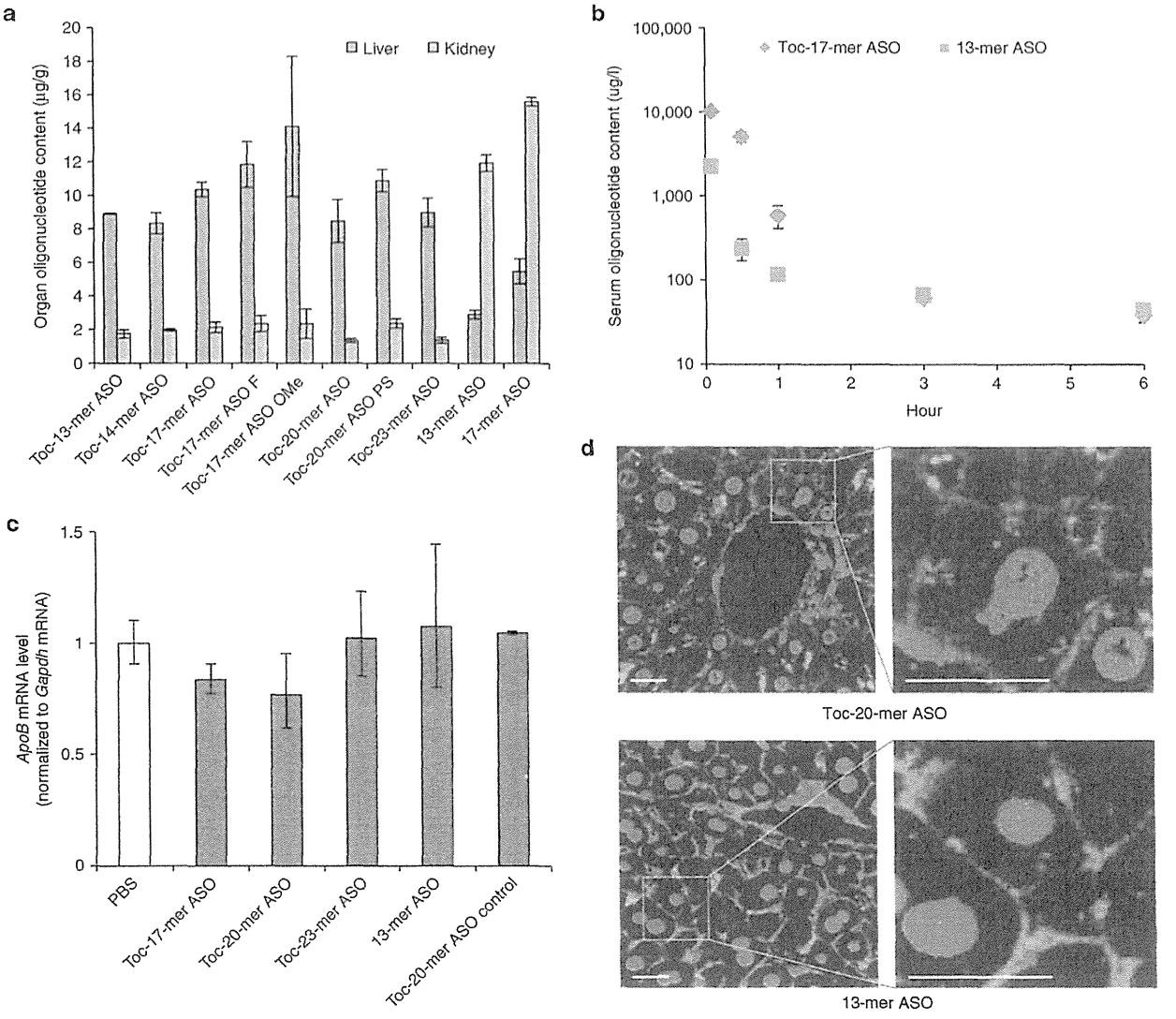

Figure 4 Biodistribution and pharmacokinesis of Toc-ASO. (**a**) Measurement of ASO concentrations in each organ 6 hours after injection of 3 mg/kg Alexa Fluor 647–labeled ASOs. The data shown are presented as mean values ± SEM ($n = 3$). The other organs including brain, heart, lung, spleen, intestine and muscle had no signal. (**b**) Measurement of serum ASO concentration 5 minutes to 6 hours after injection of mice with 3 mg/kg of Alexa Fluor 647–labeled ASOs. The data shown are presented as mean values ± SEM ($n = 3$). N.D., not detected. (**c**) Quantitative RT-PCR analyses of *Apolipoprotein B* (*ApoB*) mRNA levels relative to *gapdh* mRNA levels in the intestine 3 days after injection of 3 mg/kg Toc-ASOs. The data shown are relative to those from mice that received PBS alone and are presented as mean values ± SEM ($n = 3$). (**d**) Confocal laser images of mouse liver sections taken 6 hours after injection of 3 mg/kg Alexa Fluor 647–labeled Toc-ASOs. Red, Alexa Fluor 647–labeled ASO; green, Alexa Fluor 488 Phalloidin; blue, Hoechst 33342; Bar = 20 μm.

(Figure 4a). No accumulation of Toc-ASOs or α-tocopherol–unconjugated ASOs was observed in brain, heart, lung, spleen, intestine, and muscle because of under detection limit. These results suggest the predominantly delivery of Toc-ASOs to liver after intravenous injection compared to α-tocopherol–unconjugated ASOs.

Figure 4b shows the serum concentration-time profiles of Toc-17-mer ASOs and 13-mer ASO after intravenous injection in mice (3 mg/kg). The serum concentration of Toc-17-mer ASOs was greater at 5, 30, and 60 minutes after injection than that of 13-mer ASO in mice while there is no difference at 3 hours after injection between serum concentrations of Toc-17-mer ASOs and 13-mer ASO in mice. As shown in Table 2, the area under the serum concentration-time curve (AUC) of Toc-17-mer ASOs was 4.21-fold greater than that of 13-mer ASO in mice. Total body clearance (CLtot), mean residence time (MRT), steady-state volume of distribution (Vdss) and initial elimination rate constant (K_α) of Toc-17-mer ASOs was lower than that of 13-mer ASO in mice (Table 2). There is no significant change of the terminal elimination rate constant (K_β) between Toc-17-mer ASOs and 13-mer ASO in mice. These results suggested systemic clearance of Toc-17-mer ASO was significantly reduced compared to α-tocopherol–unconjugated ASOs 13-mer ASO, and

Table 2 Pharmacokinetic parameters of Toc-17-mer ASO and 13-mer ASO after 3 mg/kg intravenous administration

	Toc-17-mer ASO	13-mer ASO
AUC(∞) μg/ml·minute	379±14**	90±11
CLtot (ml/minute/g)	0.0079±0.0005**	0.0374±0.0025
MRT (minute)	32±1**	165±30
Vdss (ml/g)	0.252±0.023**	6.12±0.76
K_α (minute^{-1})	0.0571±0.0041**	0.1200±0.0111
K_β (minute^{-1})	0.00272±0.00137	0.00303±0.00052

The pharmacokinetic parameters were determined by model-independent moment analysis according to experimental procedures.
AUC, area under the serum concentration-time curve; CLtot, total body clearance; MRT, mean residence time; K_α, initial elimination rate constant; K_β, terminal elimination rate constant; Vdss, steady-state volume of distribution.
$n = 3$, $^{**}P < 0.01$, significantly different between Toc-17-mer ASO and 13-mer ASO.

Toc-17-mer ASO was delivered to liver from the serum more than that of 13-mer ASO in mice (Table 2).

Since *ApoB* mRNA was expressed in the intestinal tract, we measured the *ApoB* mRNA silencing effect of Toc-ASOs in intestine. Toc-ASOs had no silencing effect of target gene in intestine even injected 3 mg/kg to the mice (Figure 4c). We also examined the delivery to the liver histologically. We found much more intense Alexa Fluor 647 signals in the cytosol of hepatocytes as well as in the sinusoids of mice injected with Toc-20-mer ASO than in those of mice injected with 13-mer ASO (Figure 4d).

Phenotypic analyses of mice using α-tocopherol–conjugated ASOs

The reduction in liver *ApoB* mRNA led to a decrease in serum LDL-cholesterol level. Injection of Toc-17-mer ASO or Toc-20-mer ASO achieved a significant reduction in serum LDL-cholesterol and total cholesterol levels (Figure 5a). Western blot analysis of the sera also revealed a clear decrease in ApoB100 content by administration of Toc-17-mer ASO and Toc-20-mer ASO than 13-mer ASO (Figure 5b).

Lack of side effects of α-tocopherol–conjugated ASOs

Biochemical analysis of the serum transaminases 3 days after injection of 3 mg/kg ASOs (Figure 6a) revealed no marked abnormalities. In addition, no histological abnormalities were found in the livers of 3 mg/kg Toc-17-mer ASO–injected mice (Figure 6b).

Discussion

We previously showed that conjugation of α-tocopherol to siRNA (Toc-siRNA) improves the gene silencing effect of this construct *in vivo*;[17] however, here, we found that the direct conjugation of α-tocopherol to ASO (Toc-13-mer ASO) abolished this ability (Figure 2a). Because we observed more accumulation of Toc-13-mer ASO than of α-tocopherol–unconjugated 13-mer ASO in the liver (Figure 4a), we thought that α-tocopherol attenuated the effect of ASO in the hepatocytes. We therefore inserted second wing between the 5′-end of the ASO and the α-tocopherol to avoid α-tocopherol influence. We chose PEG (hexaethylene glycol) or second wings of nucleic acid analogues (*e.g.*, UNA, 2′-F RNA or

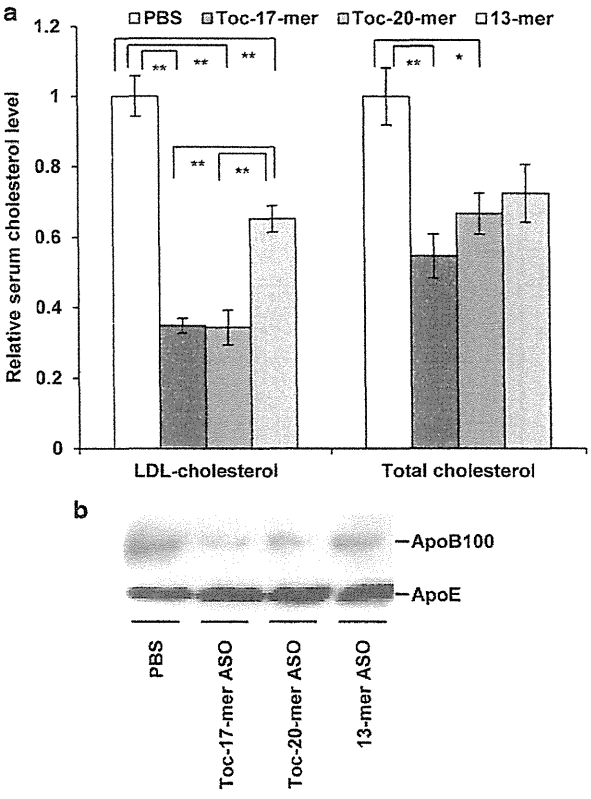

Figure 5 Phenotypic changes in lipid metabolism caused by inhibition of liver *ApoB* mRNA expression. (**a**) Decreased levels of serum low density lipoprotein cholesterol (LDL-cholesterol) and total cholesterol after injection of Toc-ASOs. Sera were collected from mice 3 days after the injection of Toc-ASOs. The resultant ratios were normalized against values from mice that were treated with PBS alone. $n = 3$, data shown are mean values ± SEM. $^{*}P < 0.05$, $^{**}P < 0.01$ compared with the PBS group. (**b**) Western blot analysis to detect serum ApoB100 proteins in mouse serum 3 days after injection.

2′-*O*-methyl RNA) as linkers. Whereas Toc-13-mer, Toc-13-mer PEG, and Toc-20-mer ASO PS had no effect, inserting the second wing of nucleic acid analogues with a natural phosphodiester internucleotide linkage produced a profound gene slicing effect (Figure 2a).

Northern blot analysis of the liver from effective Toc-ASO groups showed 13-mer bands (Figure 2d,e). Toc-13-mer ASO, Toc-13-mer ASO PEG, and Toc-14-mer ASO could not be observed in northern blot analysis, even though it was certain that the nucleic acids had reached the liver at 6 hour after injection as same amount as Toc-17-mer ASO or Toc-20-mer ASO from the fluorescence measurement (Figure 4a). This may have been because the conjugated α-tocopherol inhibited the hybridization of the ASO and the target mRNA when α-tocopherol was too close to the ASO. This clearly indicated that the 13-mer ASO was separated from α-tocopherol by cleavage of the second wing portion, suggesting that silencing of the Toc-ASOs may have been brought about by these cleaved 13-mer ASOs. ASOs bound to α-tocopherol via UNA were not degraded in mice serum (Figure 3c). α-tocopherol and second wings of Toc-ASOs were suggested to be cleaved

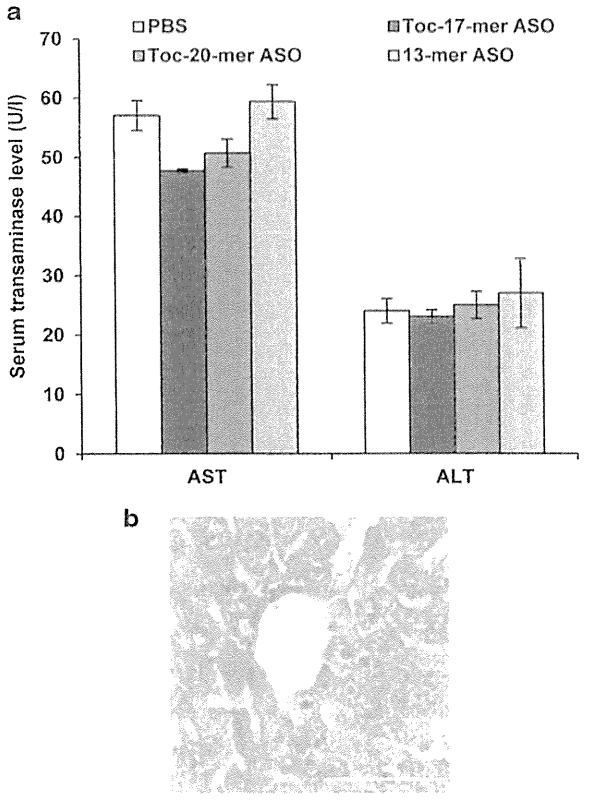

Figure 6 Evaluation of adverse events. (**a**) Serum transaminase levels 3 days after injection of 3 mg/kg Toc-ASOs. $n = 3$, data shown are mean values ± SEM. (**b**) Histopathological analyses of liver from Toc-ASO-injected mouse. Liver sections were prepared 3 days after injection of 3 mg/kg Toc-20-mer ASO.

into 13-mer ASO in mice liver (Figure 3d). The high effectiveness of Toc-ASOs in liver appears to be dependent on their high-level, *in vivo* delivery to the liver by α-tocopherol and release from α-tocopherol after uptake by the hepatocytes.

Tissue distribution and pharmacokinetic of Toc-17-mer ASO is different from that of 13-mer ASO (Figure 4a,b). Toc-17-mer ASO was predominantly distributed to liver in mice after intravenous injection. The CLtot of Toc-17-mer ASO was significantly reduced in mice compared to that of 13-mer ASO. These findings suggested that conjugation of α-tocopherol significantly improved the pharmacokinetic profile of ASO.

Toc-13-mer PEG's linker, hexaethylene glycol, was designed to be similar in length to that of the 7-mer oligonucleotide second wing of Toc-20-mer ASO. Both probably uncleaved Toc-13-mer PEG and Toc-20-mer ASO PS (Toc-ASOs with phosphodiesterase-resistant second wings) had no gene-silencing effects, indicating that α-tocopherol conjugation inhibited the effect of the ASO and that merely introducing space between α-tocopherol and the 13-mer ASO does not improve the silencing effect of Toc-ASOs.

Conjugation of α-tocopherol barely changed the *Tm* values of Toc-ASOs (Table 1), indicating that α-tocopherol conjugation did not markedly affect the duplex formation of ASO with the target mRNA *in vitro*. However, *in vivo*, the high hydrophobicity of α-tocopherol may have impeded gene silencing by interfering with the Toc-ASO's access to the target RNA during its intracellular trafficking by either binding to the membranes of intracellular organelles or intracellular proteins or inhibiting the function of proteins necessary for gene expression (including RNase H), or both.

Toc-17-mer ASO with the UNA second wing was more effective than Toc-17-mer ASO OMe or Toc-17-mer ASO F (Figure 2a). Since the arrival amounts to the liver of Toc-17-mer ASO, Toc-17-mer ASO OMe, or Toc-17-mer ASO F were not different so much (Figure 4a), the difference of the effects are not considered to be due to the quantity in the liver. Northern blot analysis showed a band signal for the 13-mer ASO in the sample containing the Toc-17-mer ASO with the UNA second wing (Figure 2d), and it suggested that the UNA second wing with phosphorothioate bond was more easily cleaved than the 2′-*O*-Me or the 2′-F second wing in hepatocytes.

When we consider the relationship between the efficiency of the Toc-ASO with the phosphate-bound UNA second wing and the length of the second wing, we see that the efficiency was highest for the Toc-17-mer ASO and attenuated for the Toc-ASO with the longer second wing. In contrast, the Toc-14-mer ASO was not effective (Figure 2b). Given that we did not observe a 13-mer band in the northern blot with the Toc-14-mer ASO (Figure 2d), it may be that the Toc-14-mer ASO's α-tocopherol was not cleaved from the ASO. Therefore, a single UNA may not be enough to be recognized by nucleases. We thought of three possible reasons why the longer second wing attenuated the Toc-ASO's efficacy: (i) it took more time to cleave the longer second wing and (ii) the longer second wing became an obstacle for recognition by the phosphodiesterase.

The RNase H cleavage–mediated silencing mechanism of the gapmer ASO dramatically improved the effectiveness of the ASO. The nucleotide analogues that served as wings (Figure 1), such as LNA, MOE, or cET, have been investigated to further increase the effectiveness of the gapmer. Optimization of gapmers (the length of the gap and the wings) has been shown to increase their effectiveness; the wing-gap-wing gapmer nucleotide composition of 2-8-3 or 2-8-2 in the LNA,[13] 5-10-5 (Mipomersen) in MOE,[12] and 3-10-3 in cET[19] were all reported to be excellent. We used the 2-8-3 13-mer ASO, which was one of the most effective LNA-containing gapmers. However, because the amount of unconjugated 13-mer ASO that reached the kidney was higher than that reaching the liver, the 13-mer ASO could not fully exert a sufficient effect in the liver, the target organ (Figure 4a). Here, we succeeded in improving the amount of ASO delivered to the liver by binding a delivery molecule to the ASO.

There have been several recent reports of organ-specific delivery of molecules conjugated to siRNA, including cholesterol to the liver[20] or brain capillary endothelial cells,[21] GalNac to the liver,[22] atelocollagen to the liver,[23] dynamic polyconjugates to the liver,[24] peptide derived from rabies virus glycoprotein to neurons,[25] and oligo-9-arginine peptide to T cells,[26] as well as the delivery of peptide conjugated to phosphorodiamidate morpholino oligomers to skeletal muscle.[27] Recently,

Prakash *et al.* reported GalNac conjugated to ASO with linker, and the GalNac-conjugated ASO improved potency in mouse liver resulted in enhanced ASO delivery to hepatocytes.[28] The GalNac-conjugated ASO is metabolized to liberate the parent ASO in the liver,[28] similar to Toc-ASO.

Our chimeric ASO with the appropriately cleavable second wing can be applied to different organs or cells by selecting different delivery molecules. Further improvements of the molecule design of the second wing will help further potency and safety for the clinical application of this new type of chimeric oligonucleotide.

Materials and methods

Design and synthesis of ASOs. A series of DNA-LNA gapmers of different lengths (13- to 23-mers) were designed to target mouse *ApoB* mRNA (NM_009693).[13] The ASOs were synthesized by Gene Design (Osaka, Japan). The sequences of the ASOs targeting *ApoB* mRNA were as follows: 13-mer ASO, 5′-G*C*a*t*t*g*g*t*a*t*T*C*A-3′; Toc-13-mer ASO PEG, 5′-**X***PEG*G*C*a*t*t*g*g*t*a*t*T*C*A-3′; Toc-13-mer ASO, 5′-**X**G*C*a*t*t*g*g*t*a*t*T*C*A-3′; 14-mer ASO, 5′-*A*G*C*a*t*t*g*g*t*a*t*T*C*A-3′; Toc-14-mer ASO, 5′-**X***A*G*C*a*t*t*g*g*t*a*t*T*C*A-3′; 17-mer ASO, 5′-*UCCA*G*C*a*t*t*g*g*t*a*t*T*C*A-3′;Toc-17-merASO,5′-**X***UCCA*G*C*a*t*t*g*g*t*a*t*T*C*A-3′; Toc-17-mer ASO F, 5′-**X***UCCA*G*C*a*t*t*g*g*t*a*t*T*C*A-3′; Toc-17-mer ASO OMe, 5′-**X**UCCAG*C*a*t*t*g*g*t*a*t*T*C*A-3′; Toc -20-mer ASO PS, 5′-**X***A*A*G*U*C*C*A*G*C*a*t*t*g*g*t*a*t*T*C*A-3′; 20-mer ASO, 5′-*AAGUCCA*G*C*a*t*t*g*g*t*a*t*T*C*A-3′; Toc-20-mer ASO, 5′-**X***AAGUCCA*G*C*a*t*t*g*g*t*a*t*T*C*A-3′; and Toc-23-mer ASO, 5′-**X***AUAAAGUCCA*G*C*a*t*t*g*g*t*a*t*T*C*A-3′. The shuffle sequence of the ASO targeting *ApoB* mRNA was as follows: Toc-17-mer ASO shuffle, 5′-**X***UCCAC*G*a*t*t*g*g*t*a*t*C*G*C; The sequence of the ASO targeting human *TTR* mRNA (NM_000371) was as follows:Toc-20-mer ASO control,5′-**X***TGTTTTA*T*G*t*c*t*c*t*g*c*c*T*G*G-3′; The sequence of the ASO targeting SRB1 mRNA (NM_000371) was as follows: Toc-17-mer ASO control, 5′-**X***GCUUC*A*g*t*c*a*t*g*a*c*T*T*C-3′; where the asterisks represent phosphorothioate linkages, the upper case boldface letter X represents α-tocopherol, the upper case italicized letters represent UNA, the lower case letters represent DNA, the underlined characters represent 2′-*O*-methyl sugar modification, the underlined upper case italicized letters represent 2′-Fluoro modification, and the upper case letters represent LNA (capital C denotes LNA methylcytosine). Alexa Fluor 647 fluorophores were covalently bound to the 3′-ends of the ASOs, and α-tocopherol was covalently bound to the 5′-ends of the ASOs.

UV melting analyses. UV absorbance versus temperature profile measurements were performed with an eight-sample cell changer, in quartz cells of 1-cm path length. The variations with temperature in the differences in UV absorbance measured at wavelengths of 260 nm and 320 nm were monitored. The samples containing the oligonucleotides with the complementary RNA, 5′-ugaauaccaaugcuggacuuuauaaccaatc-3′, (1.25 μmol/l in PBS) were first rapidly heated to 90 °C, maintained at 90 °C for 10 minutes, and then allowed to cool to 0 °C at a rate of 0.5 °C/minute. These samples were then left at 0 °C for 30 minutes, and the dissociation was recorded by heating to 90 °C at a rate of 0.5 °C/minute.

Mouse studies. Wild type Crlj:CD1 (ICR) mice or C57BL/6 mice aged 4–5 weeks (Oriental Yeast, Tokyo, Japan) were kept on a 12-hour light/dark cycle in a pathogen-free animal facility with free access to food and water. ASOs were administered to the mice via tail vein injection based upon body weight (0.75–6 mg/kg). All oligonucleotides were formulated in PBS, which also served as the control. The oligonucleotides were administered via either a single injection or repeated injections. All animal experiments were performed with more than three mice, and all procedures were carried out according to Tokyo Medical and Dental University's ethical and safety guidelines for animal experiments (#0140144A). Sera were collected 3 days after the final injection to measure LDL-cholesterol levels and for western blot analysis. For postmortem analyses, mice were deeply anesthetized with intraperitoneally administered 60 mg/kg pentobarbital and then sacrificed by transcardiac perfusion with PBS after confirming the absence of the blink reflex.

Quantitative real-time polymerase chain reaction. Total RNA was extracted from mouse liver or intestine by using Isogen (Nippon Gene, Tokyo, Japan). To detect mRNA, DNase-treated RNA (2 μg) was reverse-transcribed with SuperScript III and Random Hexamers (Life Technologies, Carlsbad, CA). To detect short RNAs, including DNA-LNA gapmer, quantitative RT-PCR analysis was performed by using a TaqMan MicroRNA Reverse Transcription Kit (Applied Biosystems, Foster City, CA) and a Light Cycler 480 Real-Time PCR Instrument (Roche Diagnostics, Mannheim, Germany). The primers and probes for the DNA/LNA gapmers and mouse *ApoB*, *Gapdh* (NM_008084), *Ttr* (NM_013697), *Sod1* (NM_011434), and *Hprt* (NM_013556) genes were designed by Applied Biosystems.

Isolation of the lipoprotein fraction from serum. The LDL fraction was prepared by ultracentrifugation according to a previously published method,[21] with modification. First, a half-volume of a solution of density 1.182 g/ml was layered onto one volume of mouse serum and centrifuged for 3.6 hours at 337,000*g* at 16 °C. The half-volume of the upper solution was set aside for use in experiments as the LDL fraction.

Western blot analysis. The LDL fraction from mouse serum samples (2 μl) was diluted with 18 μl of PBS, mixed with 5 μl of Laemmli sample buffer (Bio-Rad, Hercules, CA), and then denatured at 95 °C for 2 minutes. Total proteins were separated by electrophoresis on a 5–20% gradient polyacrylamide gel (ATTO Corporation, Tokyo, Japan) and transferred onto polyvinylidene difluoride membranes. Blots were probed with goat primary antibodies against ApoE (1:500, sc-6384, Santa Cruz Biotechnology, Santa Cruz, CA) and ApoB (1:500, sc-11795, Santa Cruz Biotechnology), and then incubated with an anti-goat secondary antibody (1:2,000, sc-2020, Santa Cruz Biotechnology) conjugated with horseradish

peroxidase. Blots were visualized with SuperSignal West Femto Maximum Sensitivity Substrate (Thermo Fisher Scientific, Waltham, MA) and analyzed by use of a ChemiDoc System (Bio-Rad).

Northern blot analysis. Total RNA was extracted from mouse liver by using Isogen II (Nippon Gene). Total RNA (30 μg) was separated by electrophoresis through an 18% polyacrylamide-urea gel and transferred to a Hybond-N+ membrane (Amersham Biosciences, Piscataway, NJ). The blot was hybridized with a probe corresponding to the ASO sequence. The sequence of the probe for detecting ASO was 5′-TGAataccaatGC-3′; the lower case letters represent DNA, and the upper case letters represent LNA (capital C denotes LNA methylcytosine). The digoxigenin-ddUTP was covalently bound to the 5′-end of the ASO probe. The signals were visualized with a Gene Images CDP-star Detection Kit (Amersham Biosciences).

Evaluation of blood chemistry. A single 0.75 mg/kg dose of ASOs in PBS was injected into the tail vein of mice. Sera were collected 3 days after injection, and blood chemistry was assessed.

Nuclease stability assays. Nuclease stability assays were performed according to a previously published method[29] with a modification. Briefly, ASOs were incubated in mouse serum with protease inhibitor for 24 hours at 37 °C. RNA was extracted using Isogen II, and were examined by northern blot analysis.

Measurement of ASO concentration in each organ. Mice were injected with Alexa Fluor 647–labeled ASOs; 6 hours later, tissues were obtained from various organs (brain, heart, lung, liver, kidney, spleen, intestine, and muscle). Tissues were homogenized in 500 μl of phosphate-buffered saline (PBS, Sigma-Aldrich, St Louis, MO). The concentration of Alexa Fluor 647 was measured by using i-control (Tecan, Männedorf, Switzerland).

Plasma pharmacokinetic studies. Each mouse received a bolus intravenous injection of Alexa Fluor 647–labeled Toc-17-mer ASO or Alexa Fluor 647–labeled 13-mer ASOs into tail vein. Blood samples were collected at indicated times (5, 30, 60, 180, and 360 minutes). The serum concentration of Alexa Fluor 647 was measured by using i-control (Tecan). The plasma concentration versus time data were analyzed by MOMENT based on the model-independent moment analysis method.[30] The nonlinear least-squares regression analysis program MULTI.[31] The pharmacokinetics parameters such as area under the serum concentration-time curve (AUC), the total body clearance (CLtot), the mean residence time (MRT) and the steady-state volume of distribution (Vdss), elimination rate constants (K_α and K_β) were calculated as described previously.[32]

Histopathological analyses. For pathological analyses, mouse liver was collected 3 days after injection and then postfixed in 4% paraformaldehyde in PBS for 6 hours, embedded in paraffin, cut into 4-μm thick sections with a Leica CM 3050 S cryostat (Leica Microsystems, Wetzlar, Germany), and stained with hematoxylin and eosin (Muto Pure Chemicals, Tokyo, Japan). The slides were analyzed under an Olympus AX80 Automatic Research Photomicroscope (Olympus, Tokyo, Japan). To analyze the distribution of ASO in the liver, 0.75 mg/kg Alexa Fluor 647–labeled ASOs in PBS was injected into mouse tail veins. Mouse liver was collected 3 days after injection, fixed in 4% paraformaldehyde in PBS for 12 hours, and then snap-frozen in liquid nitrogen. Tissue sections (10 μm) were prepared with a Leica CM3050 S cryostat (Leica Microsystems). The sections were stained with Hoechst 33342 (Sigma-Aldrich) to visualize nuclei and with 13 nmol/l Alexa Fluor 488 phalloidin (Life Technologies) to visualize cell membranes. They were then analyzed under a LSM 510 confocal microscope (Carl Zeiss MicroImaging GmbH).

Statistical analysis. All data represent means ± SEM. Student's two-tailed *t*-tests were used to determine the significance of differences between two groups in quantitative RT-PCR assays, analyses of lipoprotein levels in serum and plasma pharmacokinetic studies. One-way ANOVA followed by Tukey's test were used for multiple comparisons between pairs of groups.

Acknowledgments. This study was supported by grants from the Core Research for Evolutional Science and Technology (CREST), the Japan Science and Technology Agency (JST), Japan (to T.Y.), the Ministry of Health, Labor, and Welfare, Japan (to T.Y.), and Shionogi & Co., Ltd. This work was done in Bunkyo-ku, Tokyo, Japan. The investigators received funding from Shionogi & Co., Ltd. The authors declare no conflict of interest.

1. Kole, R, Krainer, AR and Altman, S (2012). RNA therapeutics: beyond RNA interference and antisense oligonucleotides. *Nat Rev Drug Discov* **11**: 125–140.
2. Obika, S, Nanbu, D, Hari, Y, Morio, K, In, Y, Ishida, T *et al.* (1997). Synthesis of 2′-O,4′-C-methyleneuridine and -cytidine. Novel bicyclic nucleosides having a fixed C_3, *-endo* sugar puckering. *Tetrahedron Lett* **38**: 8735–8738.
3. Obika, S, Nanbu, D, Hari, Y, Andoh, J, Morio, K, Doi, T *et al.* (1998). Stability and structural features of the duplexes containing nucleoside analogues with a fixed N-type conformation, 2′-O,4′-C-methyleneribonucleosides. *Tetrahedron Lett* **39**: 5401–5404.
4. Singh, SK, Koshkin, AA, Wengel, J and Nielsen, P (1998). LNA (locked nucleic acids): synthesis and high-affinity nucleic acid recognition. *Chem Commun* **4**: 455–456.
5. Freier, SM and Altmann, KH (1997). The ups and downs of nucleic acid duplex stability: structure-stability studies on chemically-modified DNA:RNA duplexes. *Nucleic Acids Res* **25**: 4429–4443.
6. Martin, P (1995). Ein neuer Zugang zu 2′-O-Alkylribonucleosiden und Eigenschaften deren Oligonucleotide. *Helv Chim Acta* **78**: 486–504.
7. Seth, PP, Vasquez, G, Allerson, CA, Berdeja, A, Gaus, H, Kinberger, GA *et al.* (2010). Synthesis and biophysical evaluation of 2′,4′-constrained 2′O-methoxyethyl and 2′,4′-constrained 2′O-ethyl nucleic acid analogues. *J Org Chem* **75**: 1569–1581.
8. Murray, S, Ittig, D, Koller, E, Berdeja, A, Chappell, A, Prakash, TP *et al.* (2012). TricycloDNA-modified oligo-2′-deoxyribonucleotides reduce scavenger receptor B1 mRNA in hepatic and extra-hepatic tissues–a comparative study of oligonucleotide length, design and chemistry. *Nucleic Acids Res* **40**: 6135–6143.
9. Monia, BP, Lesnik, EA, Gonzalez, C, Lima, WF, McGee, D, Guinosso, CJ *et al.* (1993). Evaluation of 2′-modified oligonucleotides containing 2′-deoxy gaps as antisense inhibitors of gene expression. *J Biol Chem* **268**: 14514–14522.
10. Wahlestedt, C, Salmi, P, Good, L, Kela, J, Johnsson, T, Hökfelt, T *et al.* (2000). Potent and nontoxic antisense oligonucleotides containing locked nucleic acids. *Proc Natl Acad Sci USA* **97**: 5633–5638.
11. Jiang, K (2013). Biotech comes to its 'antisenses' after hard-won drug approval. *Nat Med* **19**: 252.
12. Crooke, ST and Geary, RS (2013). Clinical pharmacological properties of mipomersen (Kynamro), a second generation antisense inhibitor of apolipoprotein B. *Br J Clin Pharmacol* **76**: 269–276.

13. Straarup, EM, Fisker, N, Hedtjärn, M, Lindholm, MW, Rosenbohm, C, Aarup, V *et al.* (2010). Short locked nucleic acid antisense oligonucleotides potently reduce apolipoprotein B mRNA and serum cholesterol in mice and non-human primates. *Nucleic Acids Res* **38**: 7100–7111.
14. Koller, E, Vincent, TM, Chappell, A, De, S, Manoharan, M and Bennett, CF (2011). Mechanisms of single-stranded phosphorothioate modified antisense oligonucleotide accumulation in hepatocytes. *Nucleic Acids Res* **39**: 4795–4807.
15. Juliano, RL, Ming, X and Nakagawa, O (2012). Cellular uptake and intracellular trafficking of antisense and siRNA oligonucleotides. *Bioconjug Chem* **23**: 147–157.
16. Kappus, H and Diplock, AT (1992). Tolerance and safety of vitamin E: a toxicological position report. *Free Radic Biol Med* **13**: 55–74.
17. Nishina, K, Unno, T, Uno, Y, Kubodera, T, Kanouchi, T, Mizusawa, H *et al.* (2008). Efficient *in vivo* delivery of siRNA to the liver by conjugation of alpha-tocopherol. *Mol Ther* **16**: 734–740.
18. Uno, Y, Piao, W, Miyata, K, Nishina, K, Mizusawa, H and Yokota, T (2011). High-density lipoprotein facilitates *in vivo* delivery of a-tocopherol-conjugated short-interfering RNA to the brain. *Hum Gene Ther* **22**: 711–719.
19. Hung, G, Xiao, X, Peralta, R, Bhattacharjee, G, Murray, S, Norris, D *et al.* (2013). Characterization of target mRNA reduction through in situ RNA hybridization in multiple organ systems following systemic antisense treatment in animals. *Nucleic Acid Ther* **23**: 369–378.
20. Soutschek, J, Akinc, A, Bramlage, B, Charisse, K, Constien, R, Donoghue, M *et al.* (2004). Therapeutic silencing of an endogenous gene by systemic administration of modified siRNAs. *Nature* **432**: 173–178.
21. Kuwahara, H, Nishina, K, Yoshida, K, Nishina, T, Yamamoto, M, Saito, Y *et al.* (2011). Efficient *in vivo* delivery of siRNA into brain capillary endothelial cells along with endogenous lipoprotein. *Mol Ther* **19**: 2213–2221.
22. Kanasty, R, Dorkin, JR, Vegas, A and Anderson, D (2013). Delivery materials for siRNA therapeutics. *Nat Mater* **12**: 967–977.
23. Takeshita, F, Minakuchi, Y, Nagahara, S, Honma, K, Sasaki, H, Hirai, K *et al.* (2005). Efficient delivery of small interfering RNA to bone-metastatic tumors by using atelocollagen in vivo. *Proc Natl Acad Sci USA* **102**: 12177–12182.
24. Rozema, DB, Lewis, DL, Wakefield, DH, Wong, SC, Klein, JJ, Roesch, PL *et al.* (2007). Dynamic PolyConjugates for targeted *in vivo* delivery of siRNA to hepatocytes. *Proc Natl Acad Sci USA* **104**: 12982–12987.
25. Kumar, P, Wu, H, McBride, JL, Jung, KE, Kim, MH, Davidson, BL *et al.* (2007). Transvascular delivery of small interfering RNA to the central nervous system. *Nature* **448**: 39–43.
26. Kumar, P, Ban, HS, Kim, SS, Wu, H, Pearson, T, Greiner, DL *et al.* (2008). T cell-specific siRNA delivery suppresses HIV-1 infection in humanized mice. *Cell* **134**: 577–586.
27. Jearawiriyapaisarn, N, Moulton, HM, Buckley, B, Roberts, J, Sazani, P, Fucharoen, S *et al.* (2008). Sustained dystrophin expression induced by peptide-conjugated morpholino oligomers in the muscles of mdx mice. *Mol Ther* **16**: 1624–1629.
28. Prakash, TP, Graham, MJ, Yu, J, Carty, R, Low, A, Chappell, A *et al.* (2014). Targeted delivery of antisense oligonucleotides to hepatocytes using triantennary N-acetyl galactosamine improves potency 10-fold in mice. *Nucleic Acids Res* **42**: 8796–8807.
29. Lennox, KA and Behlke, MA (2010). A direct comparison of anti-microRNA oligonucleotide potency. *Pharm Res* **27**: 1788–1799.
30. Tabata, K, Yamaoka, K, Kaibara, A, Suzuki, S, Terakawa, M and Hata, T (1999) Moment analysis program available on Microsoft Excel®. *Xenobio Metab Dispos* **14**: 286–293.
31. Yamaoka, K, Tanigawara, Y, Nakagawa, T and Uno, T (1981). A pharmacokinetic analysis program (multi) for microcomputer. *J Pharmacobio-dyn* **4**: 879–885.
32. Nishida, Y, Ito, S, Ohtsuki, S, Yamamoto, N, Takahashi, T, Iwata, N *et al.* (2009). Depletion of vitamin E increases amyloid beta accumulation by decreasing its clearances from brain and blood in a mouse model of Alzheimer disease. *J Biol Chem* **284**: 33400–33408.

Spinocerebellar ataxia type 31（SCA31）の臨床像，画像所見
—Spinocerebellar ataxia type 6（SCA6）との小脳外症候の比較検討—

榊原　聡子　　饗場　郁子　　齋藤由扶子
犬飼　　晃　　石川　欽也　　水澤　英洋

臨床神経学　第54巻　第6号　別刷
（2014年6月1日発行）